Active Infrared Technique for Landmine Detection: Numerical and Experimental Results

P. Fallavollita*, S. Esposito, M. Balsi
Dipartimento di Ingegneria dell'Informazione, Elettronica e Telecomunicazioni,
"La Sapienza" University, via Eudossiana 18, 00184 Rome, Italy
Humanitarian Demining Laboratory, Cisterna di Latina, Italy
*Corresponding author: paolo.fallavollita@gmail.com

Abstract: Landmines are an open problem in many countries of the world. They cause injuries and death and no technique proposed to date guarantees fast and 100% reliable detection alone. To this purpose, at the Humanitarian Demining Laboratory of "La Sapienza" University of Rome, several solutions are being studied. In this paper, numerical simulations of a prototype thermal detection system are reported, and results compared to experimental results. COMSOL simulation allowed complete understanding of physical mechanisms involved, and parametric simulation was used for design and optimization of the system.

Keywords: infrared sensing**,** heat diffusion, landmine detection, humanitarian demining

1. Introduction

Landmines cause injuries and death, and new techniques are necessary to detect them, because the metal detector is inadequate for low-metal-content landmines, and no other technique proposed to date guarantees fast and 100% reliable detection alone, [1].
In the Humanitarian Demining Laboratory (HDL) of "Sapienza" University of Rome, located at Cisterna di Latina (Italy), [2], several techniques, whose aim is detecting anti-personnel mines and other buried objects, are under study. In particular, active technologies based on electromagnetic, [4], vibrometric, [1] and infrared [3],[5] sensing are being considered.
In this paper, the new infrared technique will be described, and numerical results will be compared with experimental results. Simulations were developed [6] with the purpose of designing and optimizing the prototype, and of estimating actual material properties indirectly.
In Section 2, we describe our infrared solution and the numerical model. In Section 3, experimental and numerical results will be compared.
In Table 1, the list of the symbols used in this paper are reported.

2. The Thermal Detector

2.1 Our Device and Principle

fig. 1. Sandbox and the cart

In fig. 1 the device used in our experiments is shown. The cart runs, at constant velocity, on two rails by means of two motors mechanically coupled by gears, and controlled by a microcontroller communicating by radio link with a computer.
In additions, the cart carries four infrared heaters and pyrometers.
Each heater (of a kind commercialized for thermoplastic applications) has 500W power. The heaters have rectangular shape and they radiate quite uniformly the illuminated area, and can be switched independently of each other. At full power (500W×4=2kW) we can deliver about 70 kW/m^2, almost two orders of magnitude larger than solar radiation (less than 1 kW/m^2).
The pyrometer, controlled by its data acquisition GUI, has a resolution equal to 0.1°C.
The cart can move over a 2.6m^3 sandbox. In order to test our device, different objects were buried, among them two TS-50 low-metal-content landmine stimulants.
The heater scans, at constant and fixed velocity, the ground surface under test, and delivers power to it, that gradually diffuses in a depth of some cm. After the heating phase, cooling takes place through the surface, and surface temperature is

recorded at one or several time lags using a contactless thermometer (pyrometer), so that a trace of temperature is obtained over a scanning line. When an object is buried under the soil, it modifies heat diffusion dynamics. In particular, explosive materials have normally lower heat diffusivity than most soils, and air gaps act nearly as insulating, up to onset of convection. Therefore, diffusion of heat downwards is prevented during heating, and cooling may be slowed down by release of heat accumulated in high-heat capacity material. Such dynamic phenomena cause a temperature anomaly to appear on the surface, that results warmer (or cooler) than where no object is buried.

2.2 Numerical Model

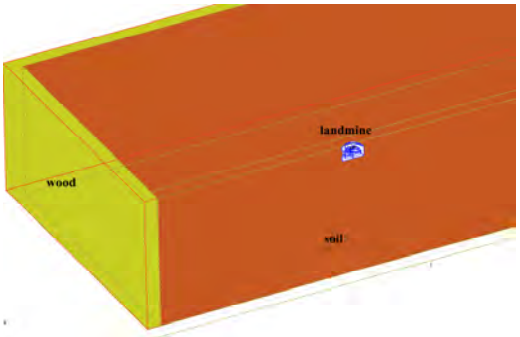

fig. 2. Integration domain.

The governing equation of the model, under the assumption of homogeneous and isotropic materials, is the energy flow equation,

$$\nabla^2 T = \frac{1}{D_i}\frac{\partial T}{\partial t} \quad (i = 1,2,3) \qquad (1)$$

where:
D_i is the object thermal diffusivity and the i-index specifies the material *(i=1)* soil, *(i=2)* landmine, and *(i=3)* wood, fig. 2. T is the temperature field, and t is the time.
The boundary and initial conditions are given in the following:

a) temperature at the top and bottom of the sandbox

$$\begin{aligned} T(x,y,z,t)\big|_{z=0,t=0} &= T_{amb} = 25(°C) \\ T(x,y,z,t)\big|_{z=-h,t=0} &= T_{bot\_ss} = 22(°C) \end{aligned} \qquad (2)$$

b) we have supposed that the soil temperature, for t=0, decreases linearly with increasing z (oriented downwards).

$$T(x,y,z,t)\big|_{\forall (x,y)\in\Re^2, t=0} = T_{amb} - (T_{amb} - T_{bot\_ss})\frac{z}{h} \qquad (3)$$

c) energy balance at the ground surface takes into account the radiant energy absorbed and emitted, and the energy exchanged with air by convective heat transfer:

$$-\vec{n}\left(-k_1\vec{\nabla}T\right) = q_0 - h_a\left(T - T_{amb}\right) - \sigma\varepsilon\left(T^4 - T_{amb}^4\right) \qquad (4)$$

where q_0 is the heat flux due to the moving heater. In this case we have considered an indoor setting, so that radiant energy is exchanged at T_{amb}. Radiant exchange with the sky would involve substantially lower reference temperature and be more significant. The absorbed heat flux q_0 was defined as following:

$$q_0 = rect_{L_x}\left(x - x_c\right) rect_{L_y}\left(y - y_c\right)\cdot p \cdot H_s(t - 0.1, 0.1) \qquad (5)$$

where $rect_L(s) = \begin{cases} 1 & |s| \le 1/2 \\ 0 & otherwise \end{cases}$

In this way we model a heat flux that vanishes everywhere, except where the heater is currently located. The heater movement was modeled by setting the coordinate of the heater center, (x_c, y_c) as function of the cart velocity, i.e.:

$$\begin{cases} x_c = vt \\ y_c = 0 \end{cases} \qquad (6)$$

In the model described here, the heater moves over the center of the buried landmine., fig. 3

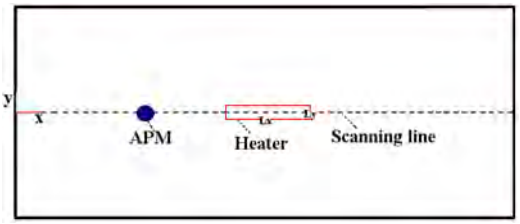

fig. 3. Heater movement geometry.

p is the specific power absorbed by unit area at the surface, defined as:

$$p = (1 - loss) \cdot \frac{P}{L_x L_y}$$

In fact, we have assumed that not all the power, P, delivered by heater, is absorbed by soil. In order to set this parameter, simulations about the heating efficiency were carried out, by comparing simulation and experimental results over free soil. In this way, we have estimated that only 55% of the power delivered by heater to the ground was absorbed.

$H_s(\cdot)$ is a smoothed Heaviside function with a continuous first derivative without overshoot, [7]. This function was necessary, in order to prevent numerical artifact due to the first kind discontinuity that would otherwise appear in eq.(5).

d) at interfaces between different materials, generically denoted by indices i and j, net heat flux is null:

$$-k_i \left.\frac{\partial T}{\partial n}\right|_i = -k_j \left.\frac{\partial T}{\partial n}\right|_j \qquad (7)$$

e) at the side surfaces of the integration domain, chosen at a sufficiently large distance from the mine, zero temperature gradient was imposed.

In order to obtain accurate numerical results around the landmine, and to reduce the computing resources required, the soil mesh was coarser than landmine mesh, as visible in fig. 4.
In order to reduce the computational burden due to limited computational resource, and to simplify the model, we have preferred to simulate the heater movement according to eq. (5) rather than using a moving mesh. In order to obtain a more accurate solution we have imposed a dense fixed mesh on the whole heated area.

All simulations were carried out using PARDISO non linear equation solver with default COMSOL configuration. In the example reported in the following, the landmine is located 1 cm under the soil surface. Thermophysical properties of materials used in this work are listed in the Table 2.

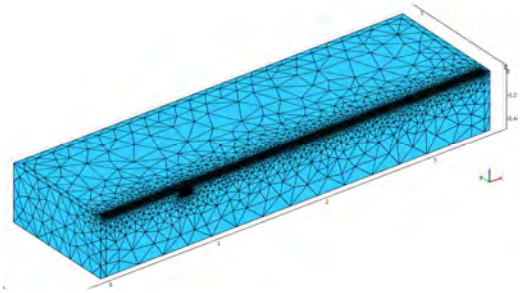

fig. 4. Soil and landmine tetrahedral mesh.

In fig. 5, the 3D model of the TS-50 landmine is shown. This model was obtained by importing into COMSOL a CAD drawing, that was obtained from public-domain technical draws of the TS-50, [8] and [9]. We have estimated that the total volume of landmine is equal to about 206cm^3 but only 0.2% of this volume is taken up by steel. This is why these landmines are called low-metal-content or plastic landmine, and are not detected by metal detectors. It is important to observe that the material that takes up the biggest part of the total volume is the air, (filling hollows necessary for the detonator to operate), because this is most relevant to the physics of heat diffusion that must be appropriately modeled in the simulation.

3. Results

Using the Heat Transfer Module of COMSOL Multiphysics, we were able to simulate the heat transfer phenomena in the soil–landmine system, and understand completely the relevant physical phenomena involved in the heating and cooling dynamics. In fact, the simulation results confirmed that the temperature anomaly produced by buried landmine is due to the differences in thermal capacity and diffusivity of the explosive material with respect to soil, and to the properties of the air contained in the mine. In order to model the latter properly, we came to the conclusion that two different regimes appear: when temperature differences are small, the low thermal conductivity of still air prevails, up the onset of convection (modeled in this work by laminar flow) inside the landmine gaps, when temperature gradient becomes large.
As the air flow is activated, heat transfer between the top side of the mine and the explosive bulk becomes significantly stronger, and cause the

latter to heat up until temperature gradients vanish and convection stops. Overall, such phenomena can be approximated by a change in thermal conductivity of air, neglecting actual modeling of air flow, that is computationally heavier.

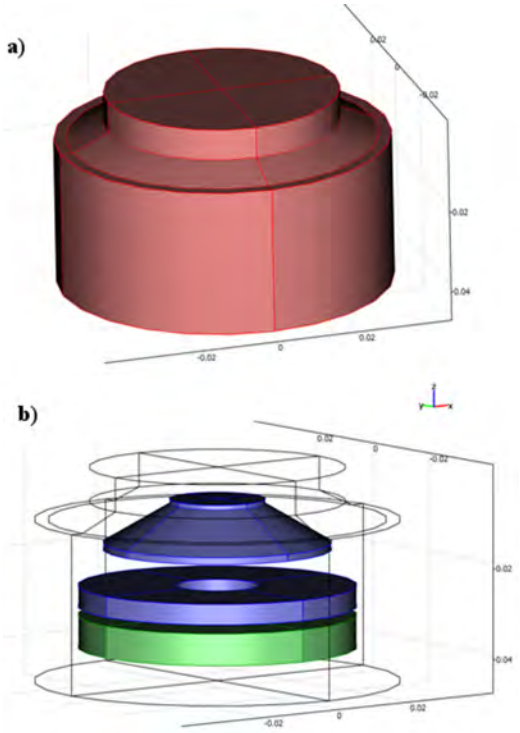

fig. 5. a) TS-50 outside geometry (plastic case). Some inessential detail was removed, to avoid drastic increase of mesh node density. b) Inside view of TS-50. Green disk is the explosive material. Blue disks are air-filled gaps. Only the striker and the pressure plate are made of steel, not visible in the figure, but taken into account in the simulations.

Therefore, we set the thermal conductivity according to eq. (8):

$$k_{eq} = \begin{cases} k_{air}\left(@\,25°C\right) & T_{top} - T_{bot} < \Delta T^{*} \\ N_u k_{air}\left(@\,25°C\right) & T_{top} - T_{bot} \geq \Delta T^{*} \end{cases} \quad (8)$$

where T_{top},(T_{bot}) ΔT^{*} and N_u are respectively the temperature at the top (bottom) of the air cavity, the threshold of temperature at which the phenomena starts, and the Nusselt Number. This approach was described in [10].

The set of the values, that produced the best fit between the simulations and measurements, were respectively 18°C for the temperature threshold and 6 for N_u.

In fig. 6 a section of the air cavity, inside the landmine, monitored in the simulation according to eq.(8) is shown. Several tests have shown that only the air cavity near the top of the landmine was interested by these phenomena. In fact, only on this cavity, the heater causes an intense temperature gradient, which enabled the described phenomena.

In the same figure it is possible to see where the T_{top} and T_{bot} were measured.

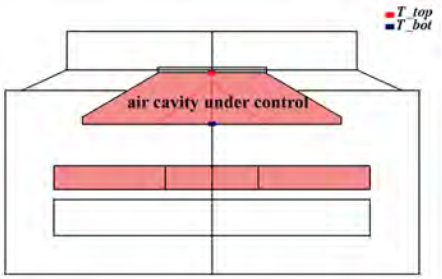

fig. 6. TS-50 cross section, the air cavity under control is visible. Red (blue) square is the point where T_{top} (T_{bot}) was measured.

It is important to underline that with these parameters, the Grashof coefficient, which is defined as ratio of the internal driving force (buoyancy force) to a viscous force acting on the fluid, [11] is less than 10^8, which is equivalent to state that the air flow is laminar rather than turbulent. This check confirms correctness of the assumption of laminar flow.

In fig. 7, a simulation is shown, where the convective heat transfer mechanism described is not implemented. Results show, that temperature over the buried landmine estimated by the simulation is larger than the measured data. This disagreement is due to the insulation effect caused by still air, which does not allow the heat to flow into deeper layers of the landmine.

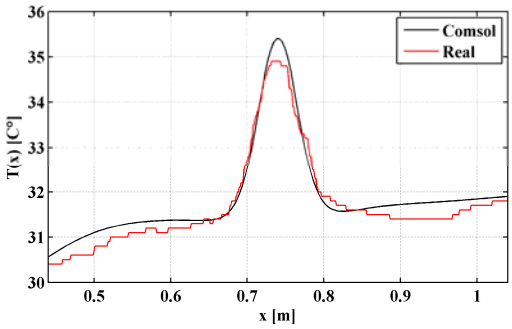

fig. 7. If air laminar flow is not taken into account in the simulations, a mismatch between them and the real data was visible.

Enabling the air laminar flow, air diffusivity increases, changing the heat transfer rate between shallow layers and the explosive bulk, and very good agreement between numerical and experimental data is obtained, fig. 8 (black line).

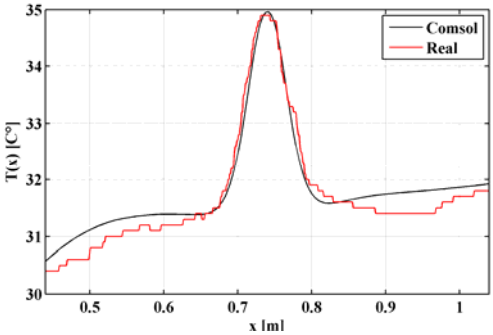

fig. 8. Numerical (black line) and experimental results (red line). Cleary a good agreement between numerical and experimental data is visible.

In figs. 9-11, a time history of the thermal diffusion process is shown. Immediately after the heating phase, fig. 5, the temperature anomaly, or APM hot-spot, is not visible yet, because at this time heat diffusion has not yet taken place, and the power delivered by the infrared heater has heated the sand surface only.
As the heat diffusion process starts, by taking the temperature profile over the soil surface around an optimum time after the heating phase, it is possible to detect the temperature anomaly. Fig. 6 shows the temperature field in the soil around the buried landmine 1500s after the heating phase; clearly a detectable thermal contrast exists. After such optimum time, the landmine continues exchanging heat, by conduction, with the soil around it, and the soil itself diffuses this heat by conduction and convection. This effect produces a thermal contrast decrease due to smoothing of the temperature distribution.

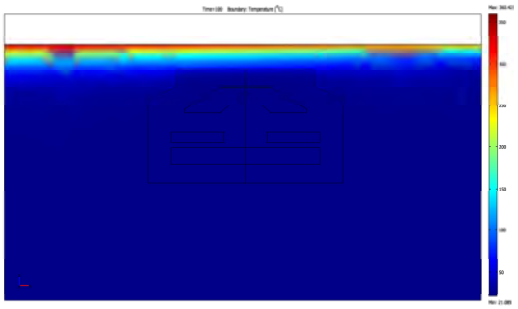

fig. 9. Temperature field of the soil around the buried landmine 100s after heating phase. At this time no thermal contrast between the landmine and soil is visible. Irregularities in temperature profile are due to relatively coarser meshing in the soil area farther from the mine.

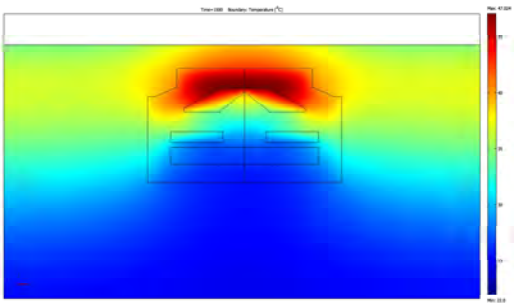

fig. 10. Temperature field in the soil around the buried landmine 1500s after heating phase. Clearly a measurable temperature difference between soil over the landmine and free soil exists; (about 5 °C).

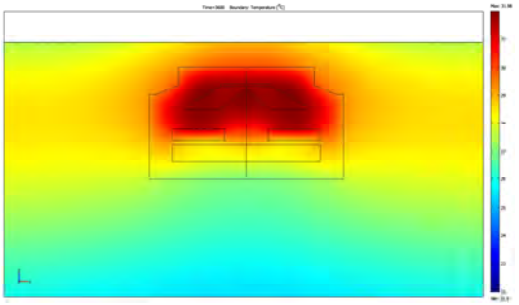

fig. 11. Temperature field in the soil around the buried landmine 3600s after heating phase. The thermal diffusion process has already taken place and the temperature of the free soil and over the buried landmine tends to become uniform.

7. Conclusions

The numerical investigation presented allowed to estimate three-dimensional transient heat diffusion fields for landmine-soil system. The very good agreement between simulated and experimental data was obtained through appropriate modeling of the heat diffusion dynamics, together with reasonable parameters obtained from literature or actual measurement, only slightly adjusted by trial and error when unknown, by checking agreement of results.

Using COMSOL, we were able to simulate the thermal phenomena for landmines buried in dry soil, understanding that landmine hot-spot was principally due to mismatches in material properties and onset of air laminar flow inside the landmine gaps.

Complete interpretation of dynamical phenomena involved in the system under study could be only qualitatively conjectured from real data. Instead, using COMSOL we were able to understand correctly what happened inside the landmine, absolutely not observable from the soil surface.

The good agreement of the simulations with experimental data permits to use this model to perform a parametric set of tests in place of time-consuming real laboratory experiments. In this way, we could optimize the system parameters (in particular: shape, size and power of the heater, and scanning speed), and the shape of the heater shield (in order to reduce heat loss by convection in air over the surface).

In fig. 12 a first example of these tests is shown. In particular we have carried out an analysis of the thermal contrast, defined as the difference between the temperature over the landmine and the temperature over free soil, for several values of the ratio between heater power and cart velocity. This ratio P/v may be interpreted as the energy absorbed by the unit length of the irradiated ground along the scanning direction.

It is interesting to observe that the higher the value of P/v ratio is, the higher the value of C is, which implies that the temperature contrast C is a direct function of P/v, rather than of P and v independently. In other words, increasing the P/v ratio, for fixed time, the contrast function increases quite linearly.

In fig. 13 a linear dependence (for fixed time and landmine depth) between thermal contrast and P/v ratio is clearly visible.

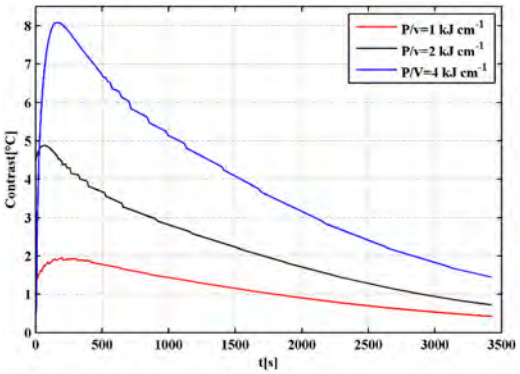

fig. 12. Contrast function for different P/v ratio. Increasing the P/v ratio, the temperature contrast increases.

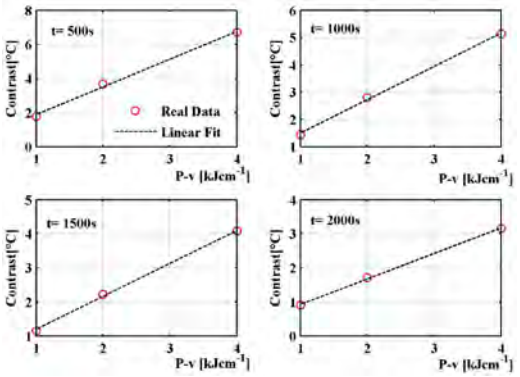

fig. 13. Contrast as P/v function. For fixed time, increasing the P/v ratio, the contrast function increases linearly.

8. Acknowledgements

We would like to thank Prof. Massimo Corcione, DIAEE of "La Sapienza" University of Rome, for his support in the model definition.

This work was supported by "Fondazione Tullio-Levi Civita", Italy, and "Tecnologie-Solidali Onlus" a non-profit organization fostering socially-oriented research and development (http://www.tecnologiesolidali.org).

References

[1] S.Esposito, *"Multi Sensor Systems for Landmine Detection"*, PhD Thesis, "La Sapienza" University of Rome 2010

[2] Laboratory website, http://w3.uniroma1.it/lsmi/hdl.htm, last access sept. 2010

[3] M. Balsi, M. Corcione, P. Dell'Omo, S. Esposito, L. Magliocchetti, "*Preliminary experimental validation of a landmine detection system based on localized heating and sensing"*, in Proc. SPIE Defense +Security, Detection and Sensing of Mines, Explosive Objects, and Obscured Targets XIII, Orlando, FL USA 16-20 March 2008, vol. 6953.

[4] M. Balsi, S. Esposito, F. Frezza, P. Nocito, P. M. Barone, S. E. Lauro, E. Mattei, E. Pettinelli, G. Schettini, C. Twizere, "*GPR Measurements and FDTD Simulations for Landmine Detection" 2010, IEEE* Proceedings of the XIII International Conference on Ground Penetrating Radar, 21-25 July 2010.

[5] Balsi M. , Corcione M. "*Thermal detection of buried landmines by local heating"* International Journal of Systems Science, Vol. 36, No. 9, 15 July 2005, 589-604

[6] M.Balsi, M.Corcione, P.Dell'Omo:*"A numerical analysis on the performance of a novel thermal scanning procedure for buried landmine detection",* WSEAS Transactions on Systems and Control, Issue 2, Vol. 1, December 2006, 1991-8763

[7] Comsol Multiphysics (2008*):"Comsol Multiphysics Reference Guide"*

[8] G. Nesti (JRC), P. Verlinde (RMA), *Joint Multi-Sensor Mine-Signature Measurement Campaign Test Protocol (MsMs-Test Protocol) Annex E Technical drawings of APL surrogates*, revised 10 March 2003 by Adam Lewis (JRC), http://demining.jrc.it/msms/protocol/annex_e.pdf last access September 2010

[9] ORDATA website http://ordatamines.maic.jmu.edu/, last access September 2010

[10] Corcione M. *"Effects of the thermal boundary conditions at the sidewalls upon natural convection in rectangular enclosures heated from below and cooled from above",* International Journal of Thermal Sciences; Vol 42, Issue 2, 2003

[11] A.Bejan, Kraus A.D.: *"Heat Transfer Handbook"*, Wiley & Sons Inc. Hoboken, New Jersey,1993.

[12] B.Sheers, M.Piette , A.Vander Vorst: *"The detection of AP mines using UWB GPR"* Second Int. Conference on the Detection of Abandoned Land Mines, October 12-14 1998

Table 1. Symbol List

ε	Soil emissivity
$\rho\ [kgm^{-3}]$	Density
σ	Stefan-Boltzman constant
$c\ [Jkg^{-1}K^{-1}]$	Specific heat
$k\ [Wm^{-1}K^{-1}]$	Thermal conductivity
$h_a\ [Wm^{-1}K^{-1}]$	Coefficient convection of air
$\vec{n}$	Direction normal at the surface
$t\ [s]$	Time
$v[cms^{-1}]$	Cart velocity
x,y,z	Cartesian Coordinates
(x_c,y_c)	Center coordinate of the heater
$D\ [m^2s^{-1}]$	Thermal diffusivity
$L_{x(y)}$	Heater dimension along x(y) direction
$P\ [W]$	Heater Power
$T\ [°C]$	Temperature
$\vec{\nabla}$	Gradient operator

Table 2. Thermophysical properties of the materials

Material	ρ	k	c
Soil, [6]	1500	0.75	781.25
Wood, [11]	500	0.14	2721
Plastic, [11]	1300	0.2	2200
Explosive,[12]	1170	0.35	836.8
Air, [11]	1.205	0.0257	1.005
Steel, [11]	7850	44.5	475